Highly sensitive microwave sensor for metallic mine detection

Maged A. Aldhaeebi, Thamer S. Almoneef
Department of Electrical Engineering, Prince Sattam Bin Abdulaziz University, Al-Kharj, Saudi Arabia

Article Info

Article history:

Received Aug 20, 2024
Revised Jan 16, 2025
Accepted Mar 3, 2025

Keywords:

High sensitivity
Metallic landmine
Microwave detecting
Scattering parameters
Sensitive sensors
Sensitivity

ABSTRACT

This study introduces an innovative microwave system for detecting buried metallic landmines, providing an alternative to conventional imaging approaches. The system consists of two highly sensitive sensors, each configured with identical antennas arranged in a triangular formation to enhance sensitivity. The proposed microwave sensors exhibit exceptional sensitivity in detecting metallic landmines buried at various depths within sand and at different distances. Simulation and experimental studies were conducted using a foam box filled with sand and a metallic cube to simulate a landmine. The sensor's sensitivity is evidenced by shifts in both the magnitude and phase of insertion loss ($S21$) between scenarios with and without a metallic mine, attributed to differences in dielectric properties between the sand and the mine in the microwave spectrum. The results from both simulations and experiments confirm the sensor's capability to detect metallic mines at varying depths within the sand medium. The proposed system offers significant advantages over imaging technologies for mine detection, including cost-effectiveness, simplicity, and ease of data processing without the need for complex imaging algorithms.

Corresponding Author:

Maged A. Aldhaeebi
Department of Electrical Engineering, Prince Sattam Bin Abdulaziz University
Al-Kharj 11942, Saudi Arabia
Email: m.aldhaeebi@psau.edu.sa

1. INTRODUCTION

Landmines are explosive devices designed to be hidden beneath the ground, waiting to be triggered by the presence or proximity of a person or vehicle. They have been used for various purposes, including military defenses, border control, and as tools of guerrilla warfare. Based on the monitor report, in 2022, a total of 4,710 individuals suffered injuries or fatalities due to landmines and explosive remnants of war (ERW) across 49 states and two additional areas including Notably, Syria and Yemen [1].

Designing a landmine detection system involves three phases: designing sensors, processing recorded data, and making decisions. The sensor design is crucial and presents several challenges, including selecting the appropriate sensor type, determining size and operating frequency, and establishing testing methods. A variety of sensors are used for mine detection, including chemical sensors [2], magnetic field loop sensors [3], and microwave sensors [4], [5].

Several techniques are used to detect landmines, such as sniffer dogs, metal detectors, acoustic sensors, electromagnetic induction, thermal imaging, and microwave detection [2], [3], [6]–[9]. Among these techniques, microwave detection based on ground-penetrating radar (GPR) offers several advantages [7], [10]. Utilizing GPR for landmine detection is widely acknowledged as an effective strategy, owing to its notable attributes such as high efficiency, directivity, and the utilization of compact sensors [8], [10].

Moreover, it is cost-effective and highly sensitive because it can penetrate the ground and provide valuable information about buried objects. This method uses electromagnetic waves that travel into the ground to interact with the subsurface and identify hidden landmines [6], [11]. The key to using electromagnetic waves for detecting buried mines lies in the differences in the dielectric properties between the sand (earth) and the materials of the mines [7]–[12].

GPR is a technology used for detecting buried landmines. It operates by sending out electromagnetic pulses into the ground and then analyzing the reflected signals to identify the presence and location of underground objects, including landmines, with a high level of accuracy. This method is known for its effectiveness, efficiency, and ability to provide valuable information about buried objects while minimizing the risk to human operators. The GPR system consists of several key components, such as a transmitter and receiver. Both transmitter and receiver are designed based on antennas that emit electromagnetic waves into the ground and receive the reflected signals [10], [13], [14].

Various types of antennas have been developed for GPR applications, including electromagnetic band-gap (EBG) [8], sinuous antenna [11], tapered slot [12], dipole [13], Vivaldi [14], [15], spiral [16], Bowtie [17], and patch antennas [18], [19]. In designing antennas for GPR, careful consideration of factors such as low profile, high efficiency, size, and cost is essential [20]–[26].

In this paper, an innovative microwave detection system developed for detecting buried metallic mines is introduced. Consisting of two highly sensitive microwave sensors, one functioning as a transmitter and the other as a receiver, the system leverages identical patch antennas arranged in triangular configurations to improve sensitivity. Through both simulation and experimental studies conducted using a foam box filled with sand and a piece of perfect electric conductor (PEC) to simulate metallic mines, we demonstrate the system's efficacy in detecting metallic landmines buried at varying depths within sand and at diverse distances. Sensitivity assessment of the sensor is accomplished by observing the shifting in both magnitude and phase of insertion loss ($S21$) between scenarios of sand devoid of mines and sand containing mines. These variations stem from disparities in dielectric properties between the sand and the metallic mines within the microwave spectrum. Both simulation and experimental results validate the sensor's adeptness in detecting metallic mines situated at different depths within the sand medium.

The other section of this paper is the following: section 2 addresses sensor modelling, designing, and simulation setup and results for modelling the ground (earth) as a foam box filled with sand and a metallic square as a mine. Also, it introduced the simulation results for two main scenarios: simulating the proposed sensor that was placed at two different distances away from the sand model box without the main and the sand model with mine inserted at various depths. Section 3 presents a measurement setup that mimics the simulation scenarios and results analysis.

2. SENSOR DESIGN AND SIMULATIONS RESULTS

The proposed sensor comprises two identical patch antennas, each accommodating four shaped triangles within a substrate of Rogress material RO4003c with a dielectric constant of 3.55 and electric tand of 0.0027 has dimensions of a length (L) equal 95.9 mm, width (W) equal 99 mm and thickness of 1.524 mm. The dimensions of each patch are 27 mm in length (ls) and 27 mm in width (ws). Additionally, each patch is loaded and connected to a small equilateral triangle with side lengths of 15 mm (lt) and a base side width of 14 mm (wt) to improve the sensitivity. To facilitate feeding, two vias are utilized to connect each patch from the bottom using coaxial feeding using CST [24], as illustrated in Figure 1(a). The proposed sensor is fabricated as depicted in Figure 1(b). FigureS 2(a) and 2(b) shows the result of the $S21$ sensor response magnitude and phase in both simulation and measurement cases.

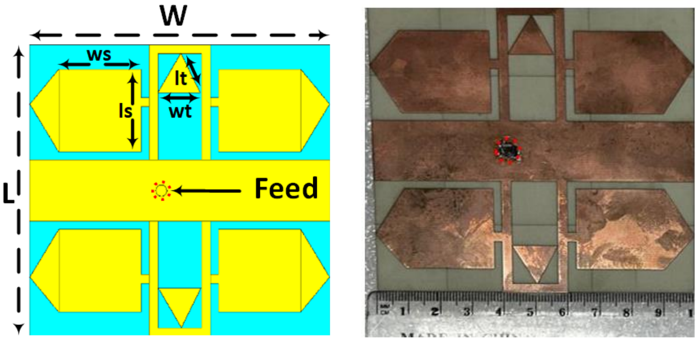

(a) (b)

Figure 1. Proposed sensor: (a) Top view in the simulation modelling and (b) Top view fabricated sensor

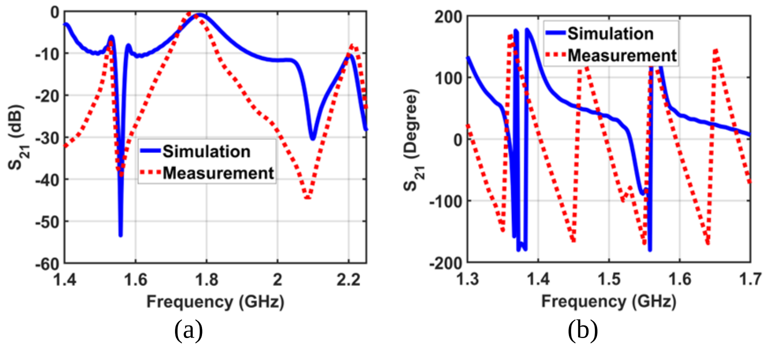

Figure 2. Simulation and measurement results of the sensor response S_{21}: (a) S_{21} in (dB) and (b) S_{21} in (degree)

In the first simulation, we aim to investigate the system's sensitivity concerning the separation between the developed sensors Tx and Rx, with three different separations denoted as SP: $SP1$ = 0 mm, $SP2$ = 20 mm, and $SP3$ = 40 mm. This simulation aims to examine the sensitivity of the proposed system when the Tx and Rx are either in close proximity or have a distance between them. In addition, to investigate the effect of the coupling data between the transmitter and receiver on the sensitivity for detecting metallic mines inserted underground as shown in Figure 3.

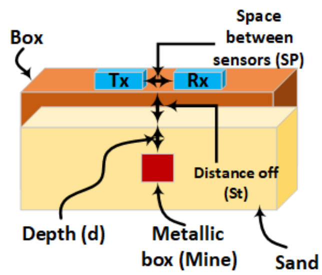

Figure 3. Simulation setup depicting the sensor enclosed within a foam box filled with sand and metallic box

In the initial procedure, the developed sensors are separated by $SP1$ = 0 mm and are positioned at a distance of $St1$= 5 mm from a foam box filled with sandy material (with a dielectric constant of 2.3 and electric tand of 0.0036), sourced from the CST library, as depicted in Figure 3. Subsequently, a metallic cube measuring 20×20×15 mm, simulating a metallic mine, is inserted at a fixed depth within the foam box, designated as $d1$ = 20 mm, to assess the sensor's performance in detecting mines at different depths. The sensor response denoted as $S21$, is recorded in both simulations, with and without the metallic cube. These simulation procedures are then repeated with the other separations between the sensors, $SP2$ 20 mm, and $SP3$ = 40 mm. All recorded data are analysed for the three separations ($SP1$ = 0 mm, $SP2$ = 20 mm, and $SP3$ = 40 mm) to determine the optimum sensor's sensitivity based on both magnitude and phase of S21 responses as illustrated in Figures 4 and 5 respectively. The results presented in Figures 4(a)-(c) and Figures 5(a)-(c), which show both the magnitude and phase of S21 at three different sensor separations (SP1 = 0 mm, SP2 = 20 mm, and SP3 = 40 mm), indicate that the highest sensitivity occurs at SP1 = 0 mm. This conclusion is based on the noticeable shifts in the magnitude and phase of the S21 response when comparing the sensor in a sandy medium without the metallic cube to the sensor in the same medium with the metallic cube.

In the next simulation, the inserted mine is investigated at three different depths inside the sand at separation $SP1$ between the Tx and Rx sensors. The developed sensor is positioned at a distance of 5 mm from a foam box filled with sandy material as illustrated in Figure 3. The simulation records the sensor responses, $S21$, in terms of both magnitude and phase. In the next step, the metallic cube is inserted at varying depths within the foam box-designated as d1, d2, and d3 (where d1 = 20 mm is the shallowest depth, d2 =30 mm is deeper than d1, and d3 =50 mm is the deepest within the sandy soil)-to evaluate the sensor's performance in detecting mines at different depths. All data regarding the sensor response $S21$ at three different depths are recorded in every analysis, inclusive of the sensor response without mine, as shown in Figures 6(a) and 6(b). The results obtained indicate that the proposed sensor successfully detects the metallic cube at all three different depths. Particularly, the sensor exhibits higher sensitivity in detecting the metallic cube at depth d1 (the closest depth to the sensor) compared to depths d1 and d3. This sensitivity is derived from the observed shifts in magnitude and phase within the sensor response $S21$ between scenarios: sensor with sandy medium without the metallic cube and sensor with sandy medium containing the metallic cube inserted at the three different depths.

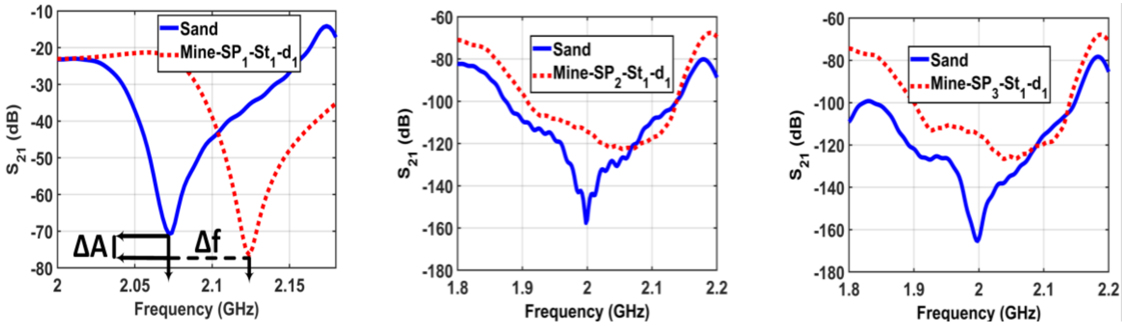

(a) (b) (c)

Figure 4. Simulation results of the magnitude sensor responses $S21$ at standoff $st1$ = 5 mm for two different scenarios: i) sandy medium without a metallic cube and ii) sandy medium with a metallic cube placed at three distinct spaces SP between the Tx and Rx sensors showing in (a) Magnitude of $S21$ (dB) at $SP1$ = 0 mm, (b) Magnitude of $S21$ (dB) at $SP2$ =20 mm and (c) Magnitude of \rssd9$S21$ (dB) at $SP3$ =40 mm

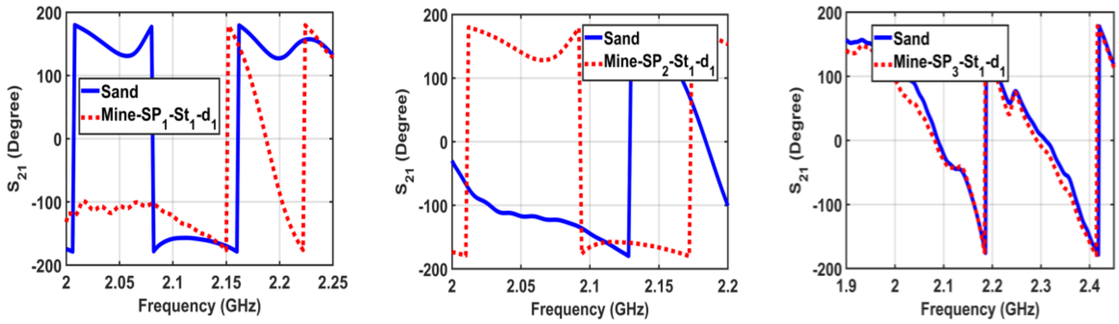

(a) (b) (c)

Figure 5. Simulation results of the phase sensor responses $S21$ at standoff $st1$ = 5 mm for two different scenarios: i) sandy medium without a metallic cube and ii) sandy medium with a metallic cube placed at three distinct spaces SP between the Tx and Rx sensors showing in (a) Phase of $S21$ (Degree) at $SP1$ = 0 mm, (b) Phase of $S21$ (Degree) at $SP2$ =20 mm and (c) Phase of $S21$ (Degree) at $SP3$ =40 mm

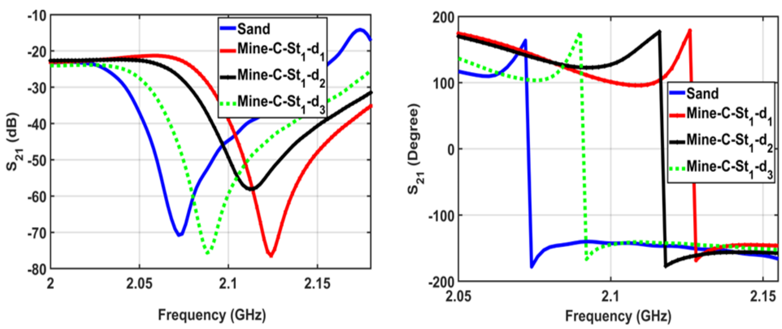

(a) (b)

Figure 6. Simulation results of the sensor responses $S21$: (a) magnitude sensor responses S_{21} and (b) phase sensor responses S_{21} at standoff $st1$ = 5 mm for two different scenarios: i) sandy medium without a metallic cube and ii) sandy medium with a metallic cube placed at three distinct depths

In the next simulations, the sensor is positioned at two different distances, $st2$ of 10 mm and $st3$ of 15 mm at $SP1$ = 0 mm, aiming to explore its sensitivity at a greater distance. The same scenarios as before, involving the sensor with a sandy medium but without the metallic cube and the sensor with a sandy medium containing the metallic cube inserted at the same three different depths, are replicated at these new distances, $st2$ and $st3$ Figures 7(a)-7(b), and Figures 8(a)-8(b) illustrate the results obtained at this second and third stand-off distances of 10 mm and 15 mm. The findings reveal that the sensor successfully detects the metallic cube at all three different depths; however, the sensor's sensitivity is observed to be lower compared to the sensitivity at the initial distance, $st1$ = 5 mm.

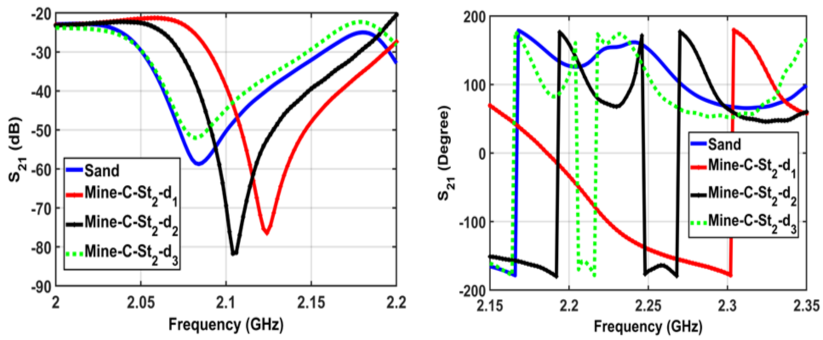

(a) (b)

Figure 7. Simulation results of the sensor responses S_{21}: (a) magnitude sensor responses S_{21} and (b) phase sensor responses S_{21} at standoff st_2 = 10 mm for two different scenarios: i) sandy medium without a metallic cube and ii) sandy medium with a metallic cube placed at three distinct depths

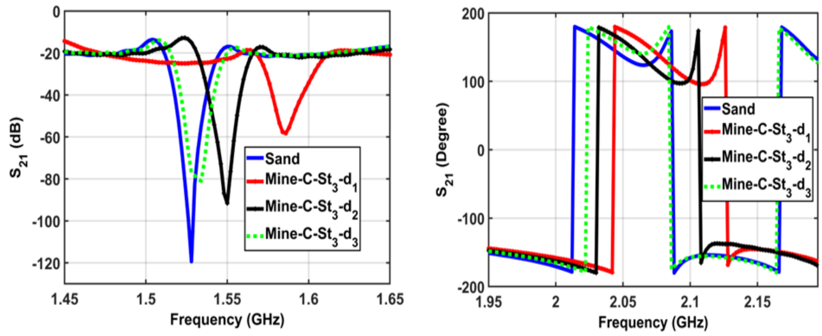

(a) (b)

Figure 8. Simulation results of the sensor responses $S21$: (a) magnitude sensor responses $S21$ and (b) phase sensor responses $S21$ at standoff $st3$ = 15 mm for two different scenarios: i) sandy medium without a metallic cube and ii) sandy medium with a metallic cube placed at three distinct depths

3. EXPERIMENT SETUP AND RESULTS

The proposed sensor undergoes fabrication and testing, as illustrated in Figures 1(b) and 2. First, experiments were carried out to validate the results obtained from simulations. The experimental setup is depicted in Figure 9, comprising a foam box filled with sand, a metallic cube, the fabricated sensor, and a vector network analyzer (VNA). In the first experiment, the separation SP between the developed sensors Tx and Rx is investigated. Three different separations denoted as SP: SP_1 = 0 mm, SP_2 = 20 mm, and SP_3 = 40 mm are utilized as shown in Figure 9. Experimental results of the above cases are shown in Figures 10(a)-10(c) and Figures 11(a)-11(c) of both magnitude and phase of S21, where the sensor's sensitivity is higher at the $SP1$ = 0 mm than in other cases of septations spaces $SP2$ = 20 mm, and $SP3$ = 40 mm.

In the next experiment, the sensor is positioned at a stand-off distance st_1 = 5 mm away from the foam box, and the sensor responses, both in magnitude and phase, are recorded. In the subsequent step, four experimental scenarios are conducted: first, the sensor with a sandy medium without the metallic cube, and in the other three experiments, the sensor with a sandy medium containing the metallic cube inserted at three different depths d1, d2, and d3 (where d1 = 20 mm, d2 =30 mm, and d3 =50 mm).

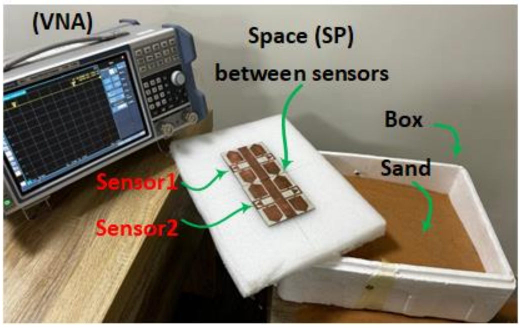

Figure 9. Experimental setup depicting the sensor enclosed within a foam box filled with sand

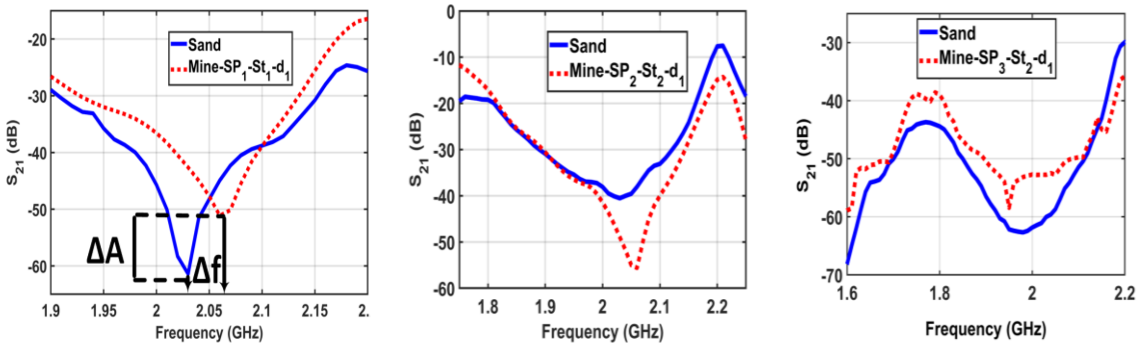

(a) (b) (c)

Figure 10. Measurement results of the magnitude sensor responses $S21$ at standoff $st1$ = 5 mm for two different scenarios: i) sandy medium without a metallic cube and ii) sandy medium with a metallic cube placed at three distinct spaces SP between the Tx and Rx sensors showing in (a) magnitude of $S21$ (dB) at $SP1$ = 0 mm, (b) Magnitude of $S21$ (dB) at $SP2$ =20 mm and (c) magnitude of \rssd9$S21$ (dB) at $SP3$ =40 mm

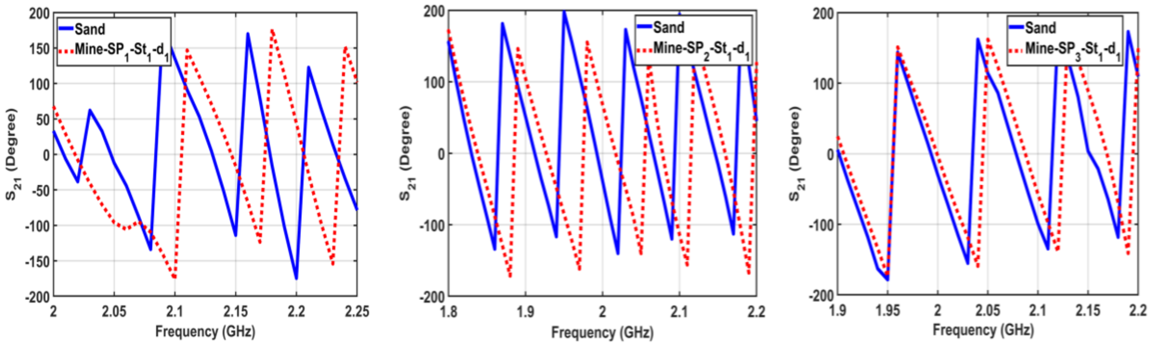

(a) (b) (c)

Figure 11. Measurement results of the phase sensor responses $S21$ at standoff $st1$ = 5 mm for two different scenarios: i) sandy medium without a metallic cube and ii) sandy medium with a metallic cube placed at three distinct spaces SP between the Tx and Rx sensors showing in (a) phase of $S21$ (Degree) at $SP1$ = 0 mm, (b) phase of $S21$ (Degree) at $SP2$ =20 mm and (c) Phase of $S21$ (Degree) at $SP3$ =40 mm

The obtained experimental results demonstrate the sensor's capability to detect the metallic cube inserted at three different depths, namely, d1, d2, and d3 as shown in Figures 12(a) and 12(b). Furthermore, the sensor exhibits higher sensitivity in detecting the metallic cube inserted at d1 (the closest depth) compared to depths d2 and d3. The sensor sensitivity is determined by observing shifts in the sensor's S_{21} response in both testing scenarios: with and without the metallic cube in the sand medium.

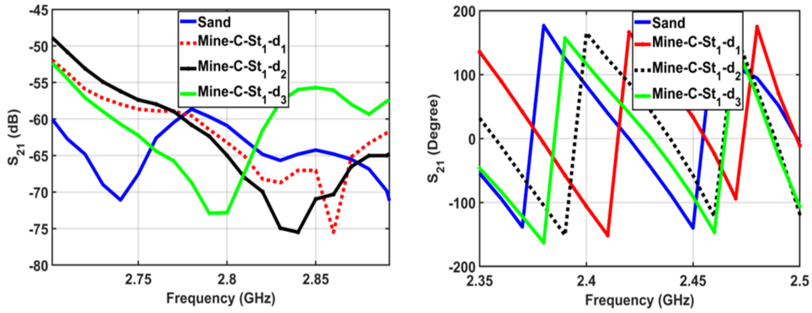

(a) (b)

Figure 12. Measurement results of the sensor responses $S21$: (a) magnitude sensor responses S_{21} and (b) phase sensor responses S_{21} at standoff $st1$ = 5 mm for two different scenarios: i) sandy medium without a metallic cube and ii) sandy medium with a metallic cube placed at three distinct depths

Another experiment was conducted to assess the sensor's sensitivity when placed at two different stand-off distances, St_2 = 10 mm and St_3 = 15 mm. This experiment replicated the same scenarios as before one with the sensor immersed in a sandy medium without the metallic cube and another with the sensor in a sandy medium containing the metallic cube inserted at the same three different depths, d1, d2, and d3. Figures 13(a)-13(b) and Figures 14(a)-14(b) show the experimental results of the sensor response S_{21} in both magnitude and phase for scenarios with and without the metallic cube. The results reveal the sensor's ability to detect the metallic cube at varying depths, d1, d2, and d3. However, the obtained results indicate that the sensor's sensitivity, as measured by the S_{21} response, is lower at the St_2 stand-off distance compared to the sensitivity observed at the St_1 stand-off distance.

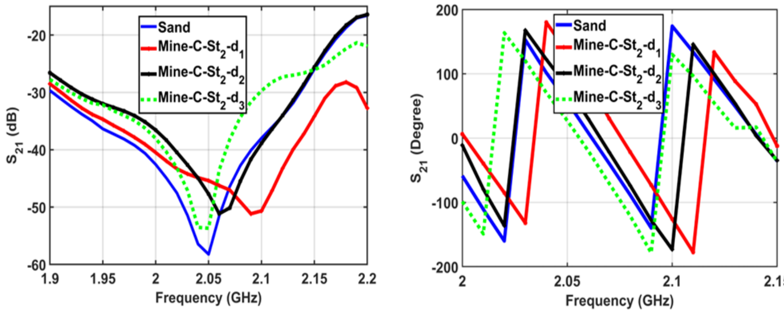

(a) (b)

Figure 13. Measurement results of the sensor responses S_{21}: (a) magnitude sensor responses S_{21} and (b) phase sensor responses S_{21} at standoff st_2 = 10 mm for two different scenarios: i) sandy medium without a metallic cube and ii) sandy medium with a metallic cube placed at three distinct depths

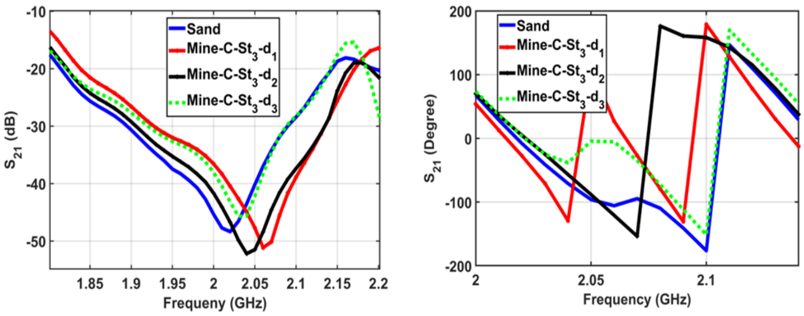

(a) (b)

Figure 14. Measurement results of the sensor responses S_{21}: (a) magnitude sensor responses S_{21} and (b) phase sensor responses S_{21} at standoff st_3 = 15 mm for two different scenarios: i) sandy medium without a metallic cube and ii) sandy medium with a metallic cube placed at three distinct depths

4. RESULTS AND DISCUSSION

GPR and microwave sensors are valuable for landmine detection, but their effectiveness varies based on the specific application and environmental conditions. GPR is known for providing detailed, high-resolution images of the subsurface and can detect landmines at different depths. However, its performance may be affected by certain soil conditions. In contrast, microwave sensors offer faster and more cost-effective detection, particularly for surface-level and near-surface landmines.

The performance of the developed microwave sensors was evaluated based on their ability to detect metallic landmines under various conditions, including different standoff distances and depths. The proposed sensors, which operate within a frequency range of 1.3 to 2.3 GHz, demonstrated high sensitivity to metal objects commonly found in landmines, such as steel. Utilizing a lower operating frequency improves penetration through sand, enhancing detection capabilities.

Additionally, the novelty of the proposed sensors lies in their structural design, where the four triangular shapes enhance sensitivity. This is attributed to the discontinuity in the top layer of the patch, which sharpens the current distribution, thereby impacting the overall input impedance of the system designed to sense the metallic mine. The current and E-field distributions results are shown in Figures 15 and 16 respectively.

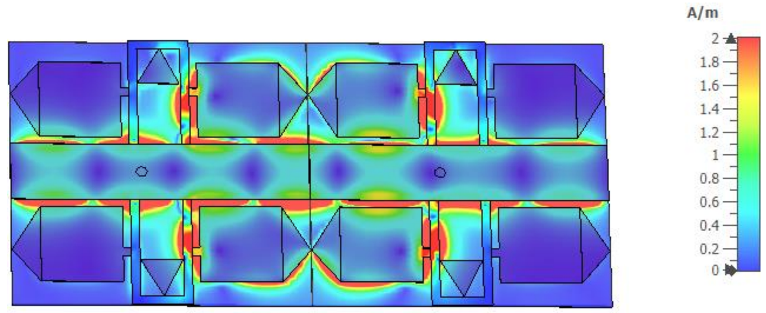

Figure 15. Simulations results shown the current distributions of proposed sensors

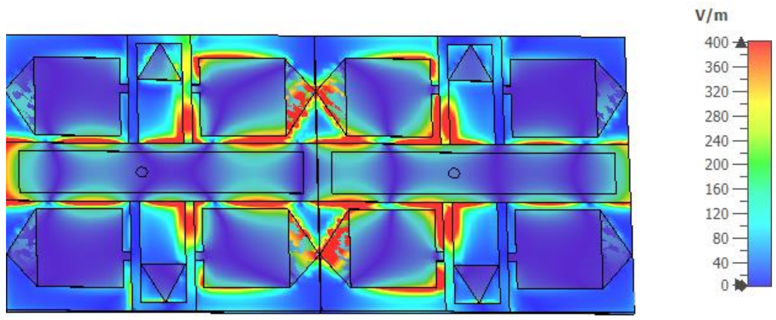

Figure 16. Simulations results shown the E-field distributions of proposed sensors

To illustrate this concept, the system's sensitivity was examined with respect to the separation distance between the developed sensors, Tx and Rx, using three distinct separation distances labelled as SP: $SP1$ = 0 mm, $SP2$ = 20 mm, and $SP3$ = 40 mm, as depicted in Figures 3 and 9. The purpose of this simulation is to assess the system's sensitivity when the transmitter (Tx) and receiver (Rx) are either in close proximity or separated by varying distances. Furthermore, this investigation aims to explore the influence of coupling between the transmitter and receiver on the sensitivity for detecting metallic mines buried underground. As shown in the results of both simulations and experiments presented in Figures 4, 5, 10 and 11 respectively, a smaller separation distance (SP) between the developed sensors Tx and Rx corresponds to a higher sensitivity for detecting metallic mines. This increased sensitivity is manifested by a more pronounced shift in both the magnitude and phase of the $S21$ parameter.

The detection depth was assessed by burying metallic land mines at three different depths: d1 = 20 mm (the shallowest), d2 = 30 mm (deeper than d1), and d3 = 50 mm (the deepest), within sandy soil, which is a typical soil composition in mine-prone regions. The sensors demonstrated a high level of accuracy in detecting mines buried up to a depth of 50 mm, as shown in Figure 6 and Figure 12 of both simulation and measuring results respectively. However, at depths greater than 50 mm, the sensitivity of the sensors decreased. Despite this, mines at a depth of 50 mm could still be detected under optimal conditions. The maximum effective detection range of the sensors was approximately 50 mm, with performance declining beyond this depth due to signal attenuation in the soil.

The performance of the microwave sensor was evaluated at two additional standoff distances-10 mm and 15 mm-to assess how the distance from the surface affects its detection capability. The experiments involved burying metallic land mine simulants under various soil types at controlled depths. At a standoff distance of 5 mm, the sensor exhibited optimal performance, demonstrating high detection accuracy characterized by significant shifts in both the magnitude and phase of the S21 parameter. The close proximity of the sensor to the target resulted in minimal signal attenuation, leading to a stronger response from the metallic targets, as shown in both simulation and experimental results in Figures 6 and 12, respectively.

At a standoff distance of 10 mm, the sensor's detection accuracy decreased slightly compared to that at 5 mm. Despite this slight reduction, the sensor remained highly effective in detecting buried mines, as shown in Figures 7 and 13 of both simulation and experimental results. At a standoff distance of 15 mm, the detection accuracy was lower than at the other standoff distances of 5 mm and 10 mm. This reduction in performance was attributed to increased signal attenuation as the distance between the sensor and the target increased, as shown in Figures 8 and 14 of both simulation and experimental results. Despite these challenges, the sensor was still able to detect larger metallic objects, though its sensitivity to smaller or deeply buried mines was reduced.

While the results indicate the microwave sensors have high potential for metallic land mine detection, there are several limitations that need to be addressed in future work. One of the primary concerns is the reduced detection accuracy at greater depths (beyond 50 mm). Further optimization of the sensor design, including the enhancement of signal processing algorithms, such as AI and the integration of multi-frequency systems, could improve the depth of detection. Additionally, efforts to miniaturize the sensor and make it more portable for use by field operatives are ongoing. The development of advanced signal processing techniques, such as machine learning algorithms to differentiate between mine-related metals and environmental clutter, would help reduce the false alarm rate even further. The microwave sensors demonstrated promising capabilities in the detection of metallic land mines, showing high sensitivity, robustness in varied environmental conditions, and an efficient operational profile compared to traditional methods. These sensors hold significant potential for improving the safety and efficiency of mine detection operations, and with further refinement, could become an invaluable tool in humanitarian demining efforts worldwide. Table 1 provides a detailed analysis of the sensor's performance and compares it with existing studies. The table compares the operating frequency, dimension and the types of used sensor, and technology principle GPR of imaging and detecting.

Table 1. Comparison between the proposed and previous studies

Reference	Frequency	Dimensions size (mm2)	Technology principle	Sensor types	Imaging or detection
[11]	0-4 GHz	100 × 100	GPR	2-sinuous antenna	Imaging
[13]	60 MHz-8 GHz	960 × 120	GPR	12-Vee dipole	Imaging
[14]	0.3-6 GHZ	NA	GPR	Vivaldi-loop	Imaging
[15]	0.4-10 GHZ	120 × 130	GPR	Vivaldi	Imaging
[16]	400- 4845 MHz	600 × 600	GPR	spiral	Imaging
[17]	0.2 GHz -1.4 GHz	340 × 510	GPR	Bowtie	NA
[18]	1.9–9.2 GHz	50 × 39	GPR	Patch	Imaging
[27]	0.98–4.5 GHz	107.7 × 68	GPR	Bow-tie	Imaging
[28]	0.18 -6.2 GHz	235 × 270	GPR	Tapered slot	Imaging
[29]	0.42–5.5 GHz	172 × 230	GPR	Bowtie	Imaging
This work	1.4-2.3 GHz	99 × 95.9	GPR	Patch	Detection

5. CONCLUSION

This paper presents an innovative microwave system developed for the detection of buried metallic landmines. The proposed system comprises two highly sensitive microwave sensors, designed based on identical patch antennas arranged in a triangular formation to enhance sensitivity. Both simulation and experimental studies were conducted using a foam box filled with sand and a metallic object that mimics a metallic mine. The system demonstrated remarkable sensitivity in detecting metallic landmines buried at various depths within the sand and at different distances. Sensitivity was determined by observing changes in both the magnitude and phase of insertion loss ($S21$) between scenarios with sand alone and sand containing a metallic mine. These variations arise from the differences in dielectric properties between the sand and the mine within the microwave spectrum. The results from both simulations and experiments confirm the system's capability to detect metallic mines at different depths in the sand medium. The proposed system offers significant advantages over imaging technologies for mine detection, including being cost effective, simple to use, and easy to process data without relying on complex imaging algorithms.

FUNDING INFORMATION

Prince Sattam bin Abdulaziz University has provided the funding for this research work through the project number (PSAU/2023/01/25942).

AUTHOR CONTRIBUTIONS STATEMENT

This journal uses the Contributor Roles Taxonomy (CRediT) to recognize individual author contributions, reduce authorship disputes, and facilitate collaboration.

Name of Author	C	M	So	Va	Fo	I	R	D	O	E	Vi	Su	P	Fu
Maged A. Aldhaeebi	✓	✓	✓	✓		✓		✓	✓	✓	✓		✓	✓
Thamer S. Almoneef	✓	✓		✓		✓	✓	✓	✓	✓	✓	✓	✓	✓

C : **C**onceptualization
M : **M**ethodology
So : **So**ftware
Va : **Va**lidation
Fo : **Fo**rmal analysis
I : **I**nvestigation
R : **R**esources
D : **D**ata Curation
O : Writing - **O**riginal Draft
E : Writing - Review & **E**diting
Vi : **Vi**sualization
Su : **Su**pervision
P : **P**roject administration
Fu : **Fu**nding acquisition

CONFLICT OF INTEREST STATEMENT

Authors state no conflict of interest.

DATA AVAILABILITY

The data that support the findings of this study are available on request from the corresponding author, MA, upon reasonable request.

REFERENCES

[1] L. S. Cumming, "International campaign to ban landmines-cluster munition coalition," in *International Encyclopedia of Civil Society*, Cham: Springer International Publishing, 2020, pp. 1–4.

[2] A. Jeremic and A. Nehorai, "Landmine detection and localization using chemical sensor array processing," *IEEE Transactions on Signal Processing*, vol. 48, no. 5, pp. 1295–1305, May 2000, doi: 10.1109/78.839977.

[3] H. Kasban, O. Zahran, S. M. Elaraby, M. El-Kordy, and F. E. Abd El-Samie, "A comparative study of landmine detection techniques," *Sensing and Imaging: An International Journal*, vol. 11, no. 3, pp. 89–112, Sep. 2010, doi: 10.1007/s11220-010-0054-x.

[4] Ping Gao and L. M. Collins, "A theoretical performance analysis and simulation of time-domain EMI sensor data for land mine detection," *IEEE Transactions on Geoscience and Remote Sensing*, vol. 38, no. 4, pp. 2042–2055, Jul. 2000, doi: 10.1109/36.851785.

[5] J. Yeo and J.-I. Lee, "High-sensitivity microwave sensor based on an interdigital-capacitor-shaped defected ground structure for permittivity characterization," *Sensors*, vol. 19, no. 3, Jan. 2019, doi: 10.3390/s19030498.

[6] D. J. Daniels, W. van Verre, F. Podd, and A. J. Peyton, "Antenna design considerations for ground penetrating radar landmine detection," *IEEE Transactions on Antennas and Propagation*, vol. 70, no. 6, pp. 4273–4286, Jun. 2022, doi: 10.1109/TAP.2022.3142309.

[7] F. Lombardi, H. D. Griffiths, M. Lualdi, and A. Balleri, "Characterization of the internal structure of landmines using ground-penetrating radar," *IEEE Geoscience and Remote Sensing Letters*, vol. 18, no. 2, pp. 266–270, Feb. 2021, doi: 10.1109/LGRS.2020.2970249.

[8] I. T. McMichael, E. C. Nallon, V. P. Schnee, W. R. Scott, and M. S. Mirotznik, "EBG antenna for GPR colocated with a metal detector for landmine detection," *IEEE Geoscience and Remote Sensing Letters*, vol. 10, no. 6, pp. 1329–1333, Nov. 2013, doi: 10.1109/LGRS.2013.2239604.

[9] Z. Shaterian, A. K. Horestani, F. Martín, and M. Mrozowski, "Design of novel highly sensitive sensors for crack detection in metal surfaces: theoretical foundation and experimental validation," *Scientific Reports*, vol. 13, no. 1, Oct. 2023, doi: 10.1038/s41598-023-45556-8.

[10] M. A. Gonzalez-Huici, I. Catapano, and F. Soldovieri, "A comparative study of GPR reconstruction approaches for landmine detection," *IEEE Journal of Selected Topics in Applied Earth Observations and Remote Sensing*, vol. 7, no. 12, pp. 4869–4878, Dec. 2014, doi: 10.1109/JSTARS.2014.2321276.

[11] D. A. Crocker and W. R. Scott, "An unbalanced sinuous antenna for near-surface polarimetric ground-penetrating radar," *IEEE Open Journal of Antennas and Propagation*, vol. 1, pp. 435–447, 2020, doi: 10.1109/OJAP.2020.3015802.

[12] T. Hirano and A. Hirose, "Wideband and low direct-coupling tapered slot antenna using electromagnetic bandgap structures," *IEEE Transactions on Antennas and Propagation*, vol. 67, no. 4, pp. 2272–2279, Apr. 2019, doi: 10.1109/TAP.2019.2891452.

[13] K. Kim, A. C. Gurbuz, W. R. Scott, Jr., and J. H. McClellan, "A multi-static ground-penetrating radar with an array of resistively loaded vee dipole antennas for landmine detection," in *Proceedings Volume 5794, Detection and Remediation Technologies for Mines and Minelike Targets X*, Jun. 2005, p. 495, doi: 10.1117/12.604145.

[14] P. Klesk, A. Godziuk, M. Kapruziak, and B. Olech, "Fast analysis of C-scans from ground penetrating radar via 3-D Haar-like features with application to landmine detection," *IEEE Transactions on Geoscience and Remote Sensing*, vol. 53, no. 7,

pp. 3996–4009, Jul. 2015, doi: 10.1109/TGRS.2015.2388713.
[15] D. N. Elsheakh and E. A. Abdallah, "Compact ultra-wideband Vivaldi antenna for ground-penetrating radar detection applications," *Microwave and Optical Technology Letters*, vol. 61, no. 5, pp. 1268–1277, May 2019, doi: 10.1002/mop.31724.
[16] I. Nicolaescu, "Improvement of stepped-frequency continuous wave ground-penetrating radar cross-range resolution," *IEEE Transactions on Geoscience and Remote Sensing*, vol. 51, no. 1, pp. 85–92, Jan. 2013, doi: 10.1109/TGRS.2012.2198069.
[17] B. Lei, S. Zheng, H. Yang, and J. Yang, "A compact broadband bowtie antenna for ground-penetrating radar applications," in *2023 IEEE 11th Asia-Pacific Conference on Antennas and Propagation (APCAP)*, Nov. 2023, pp. 1–2, doi: 10.1109/APCAP59480.2023.10469823.
[18] T. Saeidi, A. R. H. Alhawari, A. H. M. Almawgani, T. Alsuwian, M. A. Imran, and Q. Abbasi, "High gain compact UWB antenna for ground penetrating radar detection and soil inspection," *Sensors*, vol. 22, no. 14, Jul. 2022, doi: 10.3390/s22145183.
[19] D. Shi, T. Aftab, G. Gidion, F. Sayed, and L. M. Reindl, "A novel electrically small ground-penetrating radar patch antenna with a parasitic ring for respiration detection," *Sensors*, vol. 21, no. 6, Mar. 2021, doi: 10.3390/s21061930.
[20] A. Barnawi *et al.*, "A comprehensive review on landmine detection using deep learning techniques in 5G environment: open issues and challenges," *Neural Computing and Applications*, vol. 34, no. 24, pp. 21657–21676, Dec. 2022, doi: 10.1007/s00521-022-07819-9.
[21] I. Catapano, G. Gennarelli, G. Ludeno, C. Noviello, G. Esposito, and F. Soldovieri, "Contactless ground penetrating radar imaging: State of the art, challenges, and microwave tomography-based data processing," *IEEE Geoscience and Remote Sensing Magazine*, vol. 10, no. 1, pp. 251–273, Mar. 2022, doi: 10.1109/MGRS.2021.3082170.
[22] Z. Chen, X. Q. Lin, Y. H. Yan, F. Xiao, M. T. Khan, and S. Zhang, "Noncontact group-delay-based sensor for metal deformation and crack detection," *IEEE Transactions on Industrial Electronics*, vol. 68, no. 8, pp. 7613–7619, Aug. 2021, doi: 10.1109/TIE.2020.3008386.
[23] M. García Fernández, G. Álvarez Narciandi, A. Arboleya, C. Vázquez Antuña, F. L.-H. Andrés, and Y. Álvarez López, "Development of an airborne-based GPR system for landmine and IED detection: Antenna analysis and intercomparison," *IEEE Access*, vol. 9, pp. 127382–127396, 2021, doi: 10.1109/ACCESS.2021.3112058.
[24] CST, "Computer simulation technology." 2024.
[25] H. Bezzout and H. El Faylali, "Agent-based model simulation for ground penetration radar based on netlogo platform," *Indonesian Journal of Electrical Engineering and Computer Science*, vol. 26, no. 1, pp. 576–586, Apr. 2022, doi: 10.11591/ijeecs.v26.i1.pp576-586.
[26] J. Ali, N. Abdullah, R. Yahya, E. Mohd, A. Joret, and N. Katiran, "Bistatic configurational analysis of ultra-wideband antenna for detection applications," *Indonesian Journal of Electrical Engineering and Computer Science*, vol. 13, no. 2, pp. 702–707, Feb. 2019, doi: 10.11591/ijeecs.v13.i2.pp702-707.
[27] M. Joula, V. Rafiei, and S. Karamzadeh, "High gain UWB bow-tie antenna design for ground penetrating radar application," *Microwave and Optical Technology Letters*, vol. 60, no. 10, pp. 2425–2429, Oct. 2018, doi: 10.1002/mop.31392.
[28] M. M. Mohanna, E. A. Abdallah, H. M. S. El-Hennawy, and M. M. Kamel, "A novel high directive willis-sinha tapered slot antenna for GPR application in detecting landmine," *Progress In Electromagnetics Research C*, vol. 80, pp. 181–198, 2018, doi: 10.2528/PIERC17111904.
[29] K. K. Ajith and A. Bhattacharya, "A novel compact super wide band bowtie antenna for 420 MHz to 5.5 GHz operation," *IEEE Transactions on Antennas and Propagation*, vol. 66, no. 8, pp. 3830–3836, Aug. 2018, doi: 10.1109/TAP.2018.2836382.

BIOGRAPHIES OF AUTHORS

Maged A. Aldhaeebi received a B.S. degree in electrical and computer engineering from Hadhramaut University, Al-Mukalla, Hadhramaut, Yemen, in 2009, a M.A.Sc. degree in Electrical and Computer Engineering from King Saud University, Riyadh, Saudi Arabia in 2014, and a Ph.D. degree in Electrical and Computer Engineering from the University of Waterloo, Waterloo, ON, Canada, in 2020. He is currently an assistant professor with the Department of Electrical Engineering, Prince Sattam bin Abdulaziz University. He has authored or co-authored more than 30 refereed journals and conference papers. His research interests include biomedical engineering, brain tumor imaging and treatment using Hyperthermia, Intelligent Microwaves-Based Modalities for Breast Cancer Detection, artificial intelligence, antenna theory, metamaterials, and their wide range applications, metamaterial absorbers, electrically small resonators, rectennas, microwave sensors, electromagnetic energy harvesting, and machine learning for electromagnetic biomedical applications. He can be contacted at email: m.aldhaeebi@psau.edu.sa.

Thamer S. Almoneef received the B.S. degree in electrical and computer engineering from Dalhousie University, Halifax, NS, Canada, in 2009, and the M.A.Sc. and Ph.D. degrees in electrical and computer engineering from the University of Waterloo, Waterloo, ON, Canada, in 2012 and 2017, respectively. In 2012, he was appointed as a lecturer and was granted a Scholarship from Prince Sattam bin Abdulaziz University, Al-Kharj, Saudi Arabia, to pursue his Ph.D. degree studies. He is currently an associate professor with the Department of Electrical and Computer Engineering, Prince Sattam bin Abdulaziz University. He has authored or co-authored more than 35 refereed journals and conference papers. His research interests include antenna theory, metamaterials and their wide range applications, metamaterial absorbers, electrically small resonators, rectennas, microwave sensors and imagers, electromagnetic energy harvesting, and renewable energy. He can be contacted at email: t.almoneef@psau.edu.sa.